High-spin states in odd-odd ^{174}Re

S. Guo,* Y. H. Zhang, X. H. Zhou, M. L. Liu, Y. X. Guo, Y. H. Qiang, Y. D. Fang, X. G. Lei, and F. Ma
Institute of Modern Physics, Chinese Academy of Sciences, Lanzhou 730000, China

M. Oshima, Y. Toh, M. Koizumi, A. Osa, A. Kimura, and Y. Hatsukawa
Japan Atomic Energy Agency, Tokai, Ibaraki 319-1195, Japan

M. Sugawara
Chiba Institute of Technology, Narashino, Chiba 275-0023, Japan

H. Kusakari
Chiba University, Inage-ku, Chiba 263-8512, Japan

(Received 2 December 2011; revised manuscript received 25 May 2012; published 19 July 2012)

High-spin states in the odd-odd ^{174}Re have been investigated via the ^{152}Sm(^{27}Al, $5n\gamma$)^{174}Re reaction with the help of excitation function, x-γ, and γ-γ coincidence measurements. Five rotational bands have been observed and their configurations were assigned based on alignments, band crossing frequencies, electromagnetic properties, and the estimated bandhead excitation energies. Low-spin signature inversion has been identified in the two-quasiparticle bands built on $\pi h_{11/2} \otimes \nu i_{13/2}$, $\pi h_{9/2} \otimes \nu i_{13/2}$, and $\pi 1/2^-[541] \otimes \nu 5/2^-[512]$ configurations. $E2$ interband transitions were analyzed with band-mixing calculations giving information on shapes and shape driving effects for the bands of interest.

DOI: 10.1103/PhysRevC.86.014323 PACS number(s): 21.10.Re, 23.20.Lv, 21.60.Ev, 27.70.+q

I. INTRODUCTION

The interplay between the odd nucleon and its core is an interesting topic associated with nuclear rotational motion. Odd-A nuclei show many interesting high-spin phenomena, such as signature splitting, deformation driving effects, e.g., changes in deformation due to the occupation of specific orbitals by the odd nucleon, and so on. For odd-odd nuclei, the system becomes more complex due to a variety of coupling schemes among the valence nucleons and the core; some new phenomena appear such as the well-known low-spin signature inversion in a number of two-quasiparticle bands built on the $\pi h_{11/2} \otimes \nu i_{13/2}$ and $\pi h_{9/2} \otimes \nu i_{13/2}$ configurations [1–7]. The nuclei in the lighter W-Re-Os region are rather soft with respect to both the β and γ deformations. Obviously the nuclear shape can be influenced by quasiparticles that occupy orbitals with a large slope in the Nilsson diagram [8,9]. In fact, $\pi h_{9/2}$ bands of odd-Z, even-N nuclei in this region usually exhibit deformation driving effects, and those are expected in the bands of odd-odd nuclei involving this proton orbital as well. As for the neutron, the $\nu(1/2^-[521])$ band is suggested to have a larger deformation in ^{175}Os [10]. In the odd-odd nuclei around ^{175}Os, the odd neutron may occupy this $\nu(1/2^-[521])$ state. Thus, ^{174}Re seems to be a good candidate to search for deformation driving effects. In this context, our attention is focused on signature inversion and deformation driving effects in odd-odd ^{174}Re.

Prior to this work, a $I^\pi = 3^+$ state with a $\pi h_{9/2}(1/2^-[541]) \uparrow \otimes \nu(1/2^-[521]) \uparrow$ configuration was proposed for the ground state of ^{174}Re by the β^+/EC decay study of ^{174}Re [11,12]. Nevertheless, this assignment was not adopted in a recent compilation [13]. As for high-spin states, the first investigation was carried out in 1988, and five rotational bands were observed [13–15]. However, the assignments of these rotational bands to ^{174}Re deviate notably from the systematics, and several γ transition sequences can be assigned to ^{175}Re instead. Our group reinvestigated ^{174}Re via a ^{159}Tb (^{20}Ne,$5n\gamma$) ^{174}Re reaction, and a new level scheme of ^{174}Re with three rotational bands was established [16]. In this article, we report on the new experimental results on high-spin band structures in ^{174}Re populated via the ^{152}Sm(^{27}Al,$5n\gamma$)^{174}Re reaction. The high-quality data allow us to extend the level scheme of ^{174}Re significantly. Preliminary results of this work have been reported in Refs. [17,18].

II. EXPERIMENTS AND RESULTS

A. Measurements

The experiment was performed at the Japan Atomic Energy Agency (JAEA) using the ^{152}Sm(^{27}Al,$5n\gamma$) fusion-evaporation reaction. The ^{27}Al beam was provided by the JAEA tandem accelerator, with a typical beam current of 1 particle nA. The target was an enriched 2.0-mg/cm^2 ^{152}Sm metallic foil backed with a 10-mg/cm^2 Pb layer. A γ-ray detector array [19], consisting of 13 large volume High Purity Germanium (HPGe) detectors with bismuth germinate (BGO) anti-Compton shields, was used; six detectors had an efficiency of 40% each and the others had an efficiency of 70% relative to a $3'' \times 3''$ NaI scintillator. The detectors were calibrated with ^{60}Co, ^{133}Ba, and ^{152}Eu standard sources. The typical energy resolutions were about 2.0–2.5 keV at full width at half maximum for the 1332.5-keV line.

The in-beam γ rays belonging to ^{174}Re were identified by measuring an excitation function at beam energies of 125,

*gs@impcas.ac.cn

132, and 140 MeV. The γ-ray spectra in this experiment were very complex; the photon peaks were often doublets or contaminated by the γ rays from other reaction channels. We, therefore, used the coincidence mode in the excitation function measurements. At each beam energy, about 10×10^6 γ-γ coincidence events were accumulated and sorted on-line into a symmetric E_γ-E_γ matrix. The Re K x-ray gated γ-ray spectra were projected and analyzed with care during experiment. The intensities of known γ rays from ^{175}Re (^{174}W) decrease with increasing the beam energy, whereas some known ^{174}Re γ rays (from the previous work [16]) and ^{173}Re were found to have increasing intensities. This can be seen in the Re K x-ray gated spectra presented in Fig. 1(a), where the gamma rays emitted from ^{175}Re (138-, 160-, 210-, 315-, and 390-keV lines [20]) and ^{174}W (243- and 349-keV lines [13]) have been observed at a 125-MeV beam energy (upper panel) whereas the γ rays from ^{174}Re (93-, 115-, 303-, and 344-keV lines [16]) and several contaminant γ rays from ^{173}Re (indicated by the filled circles [21]) are dominant at the beam energy of 140 MeV (lower panel). A quantitative analysis is also demonstrated in Fig. 1(b). As shown in the figure, the γ rays from ^{175}Re and ^{174}W can be clearly separated from those of ^{174}Re. Thus, some unknown γ rays were assigned to ^{174}Re, such as the 188-, 388-, and 465-keV lines. It should be noted that the well-established high-spin level schemes for ^{152}Sm [22], ^{173,175}Re, ^{171}Ta [23], and ^{174}W were very useful for the assignment of new γ rays to ^{174}Re.

The γ rays from ^{174}Re are found to be predominant at the 140-MeV beam energy; therefore, the γ-γ coincidence measurement was performed at this beam energy. The time window Δt of 200 ns was set in the coincidence measurement. A total of 2×10^8 γ-γ coincidence events were accumulated and sorted into a symmetric E_γ-E_γ matrix of 4096×4096 size for the off-line analysis.

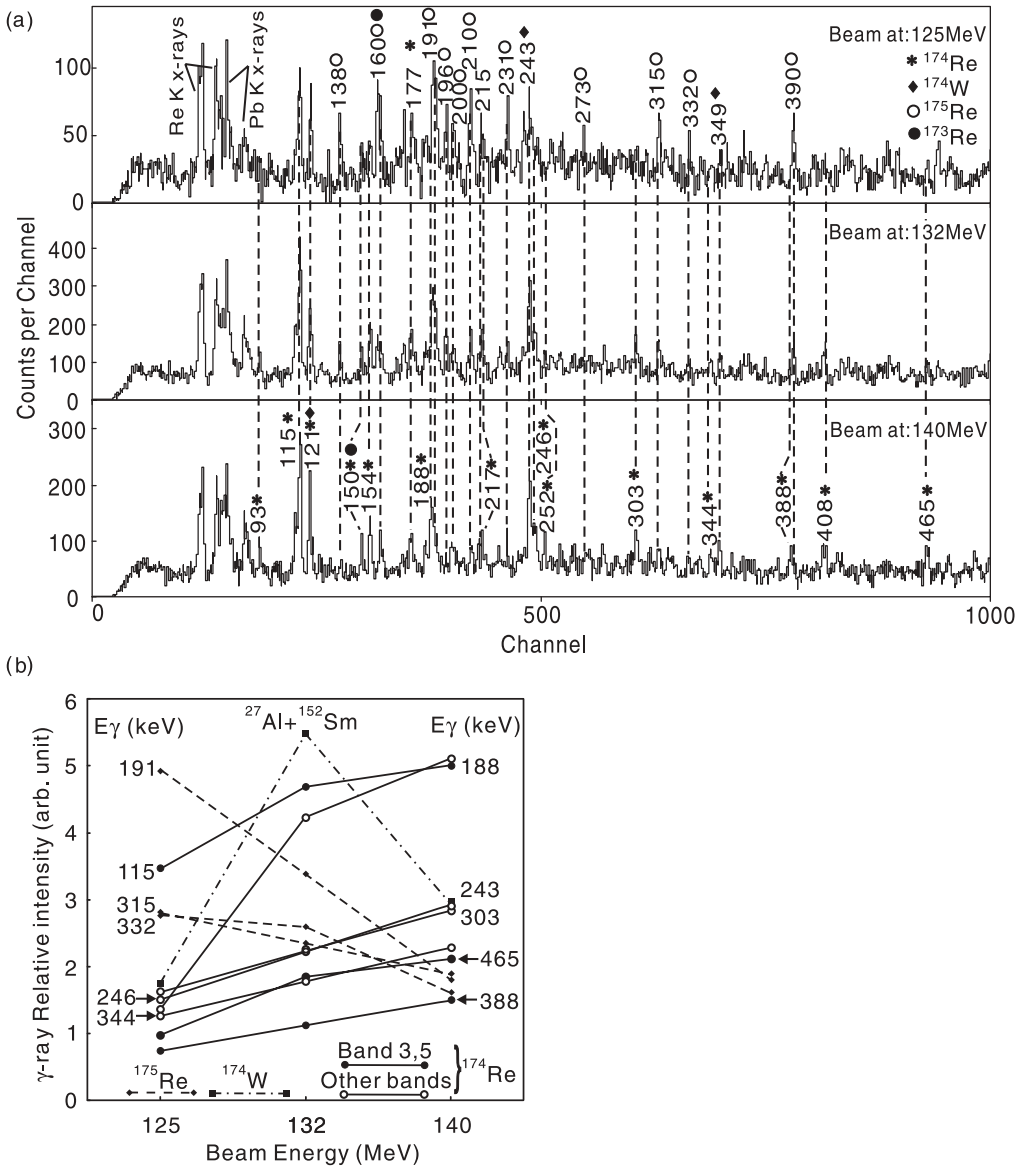

FIG. 1. (a) Re K x-ray gated spectra at 125-, 132-, and 140-MeV beam energies. (b) Intensities for some γ rays normalized to the same beam current.

To determine the multipolarities and multipole mixing ratios, δ, of the emitted γ rays, the technique of directional correlations of γ rays de-exciting oriented states (DCO) [24,25] was used. The coincidence events were sorted into an asymmetric matrix with one γ ray detected in one of the six detectors at 47 or 147° and the other one detected in one of the seven detectors close to 90° with respect to the beam direction. The experimental DCO ratio was calculated by $R_{\rm DCO}(\gamma) = I_\gamma(47\text{–}90^\circ)/I_\gamma(90\text{–}47^\circ)$, where $I_\gamma(\theta_1 - \theta_2)$ represents the intensities of the γ ray of interest along the θ_1 axis in coincidence with stretched-$E2$ transitions along the θ_2 direction. In the present geometry, stretched quadrupole transitions were adopted if $R_{\rm DCO}(\gamma)$ was close to unity, and dipole transitions were assumed if $R_{\rm DCO}(\gamma) \leqslant 0.6$. Additionally, the DCO ratio has a dependence on the $E2/M1$ mixing ratio δ and the dealignment parameter, σ/I [26]. δ values of several γ rays were, therefore, deduced from DCO ratios (see Fig. 2), using a common dealignment parameter $\sigma/I = 0.3$ [27]. In the present work, the sign of δ values follows the Krane and Steffen convention [28].

Here, the angular distribution from oriented nuclei (ADO) method was used as well. Two asymmetric coincidence matrices were constructed using the γ rays detected at all angles (y axis) against those observed at ∼47° (or 147°) and 90° (x axis), respectively. From these two matrices, the angular distribution asymmetry ratios, defined as $R_{\rm ADO}(\gamma) = I_\gamma(47^\circ)/I_\gamma(90^\circ)$, were extracted from the γ-ray intensities $I_\gamma(47^\circ)$ and $I_\gamma(90^\circ)$ in the coincidence spectra gated by the γ transitions (on the y axis) of any multipolarity. Stretched quadrupole transitions were adopted if $R_{\rm ADO}(\gamma)$ values were significantly larger than unity, and the dipole transitions were assumed if $R_{\rm ADO}(\gamma)$ values were less than 1.0.

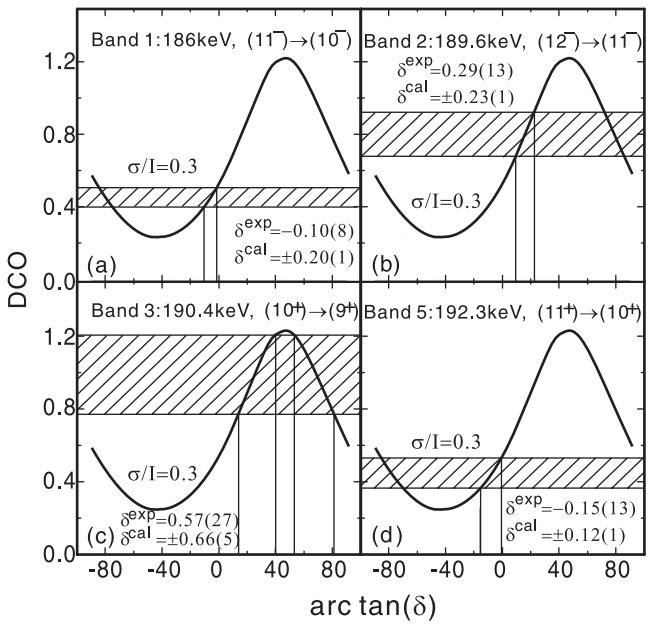

FIG. 2. Experimental calculated DCO ratios for selected transitions of (a) band 1, (b) band 2, (c) band 3, and (d) band 5. The experimental mixing ratios are indicated, with the large solutions rejected through a comparison with the results calculated by Eq. (2).

The experimental branching ratio for a given state, defined as

$$\lambda = \frac{T_\gamma(I \to I-2)}{T_\gamma(I \to I-1)}, \quad (1)$$

was obtained from relative γ-ray intensities in the coincidence spectrum gated by a γ ray located above that level.

Given the spin I, the projection quantum number K, the transition energy E in MeV, and the branching ratio, the absolute value of the mixing ratio δ can be deduced from the rotational-model expression:

$$\frac{\delta^2}{1+\delta^2} = \frac{2K^2(2I-1)}{(I+1)(I+K-1)(I-K-1)} \left(\frac{E_1}{E_2}\right)^5 \lambda. \quad (2)$$

By comparison with the results calculated by this method, the solutions for the mixing ratios derived from the DCO method are selected as demonstrated below in Fig. 2.

The branching ratio was also used to extract the ratio of reduced transition probabilities, which is defined as

$$\frac{B(M1, I \to I-1)}{B(E2, I \to I-2)} = 0.697 \frac{[E_\gamma(I \to I-2)]^5}{[E_\gamma(I \to I-1)]^3} \frac{1}{\lambda} \frac{1}{1+\delta^2} \left(\frac{\mu_N^2}{e^2 b^2}\right), \quad (3)$$

where $E_\gamma(I \to I-1)$ and $E_\gamma(I \to I-2)$ are the $\Delta I = 1$ and 2 transition energies, respectively. In the calculations, δ has been set to zero. Thus, the experimental $B(M1)/B(M2)$ ratios extracted here should be regarded as an upper limit.

B. Level scheme

The level scheme of ^{174}Re deduced in the present work is presented in Fig. 3. Bands 1, 2, 4, and 5 have been reported previously [17,18], while band 3 is presented here for the first time. Transition energies, spin assignments, γ intensities (at the beam energy of 140 MeV), branching ratios, B($M1$)/B($E2$) ratios, DCO ratios, and ADO ratios are listed in Table I for each band or pairs of linked bands.

In Fig. 4(a), the lines belonging to band 1 are indicated, obtained by gating on the 93.2-keV transition, which depopulates the band. Setting a gate on the 271.2-keV γ ray, we deduced the total conversion coefficient $\alpha_T = 4.6(4)$ for the 93.2-keV transition from the intensity balance between the 176.5 + 116.7 and 93.2-keV transitions. This value is consistent with an $M1$ or $E2$ multipolarity ($\alpha_{E1} = 0.46$, $\alpha_{M1} = 6.54$, and $\alpha_{E2} = 5.56$) [29]. The $M1 + E2$ character of the 93.2-keV transition is further supported by its DCO and ADO values (see Table I). Therefore, the 93.2-keV line is assigned to feed a state with tentative spin and parity (5^-).

Likewise, we identify γ rays from band 2 by gating on the 115.5-keV line, shown in Fig. 4(b). Again, gating on the 154.8-keV line, we analyze the intensity balance between the 205.8 + 121.1 and 115.5-keV transitions. The deduced internal conversion coefficient 0.62(10) suggests that the 115.5-keV transition has an $E1$ multipolarity, in agreement with the theoretical value of 0.27 [29]. Therefore, the 115.5-keV line is assigned to feed a (7^+) state as indicated in

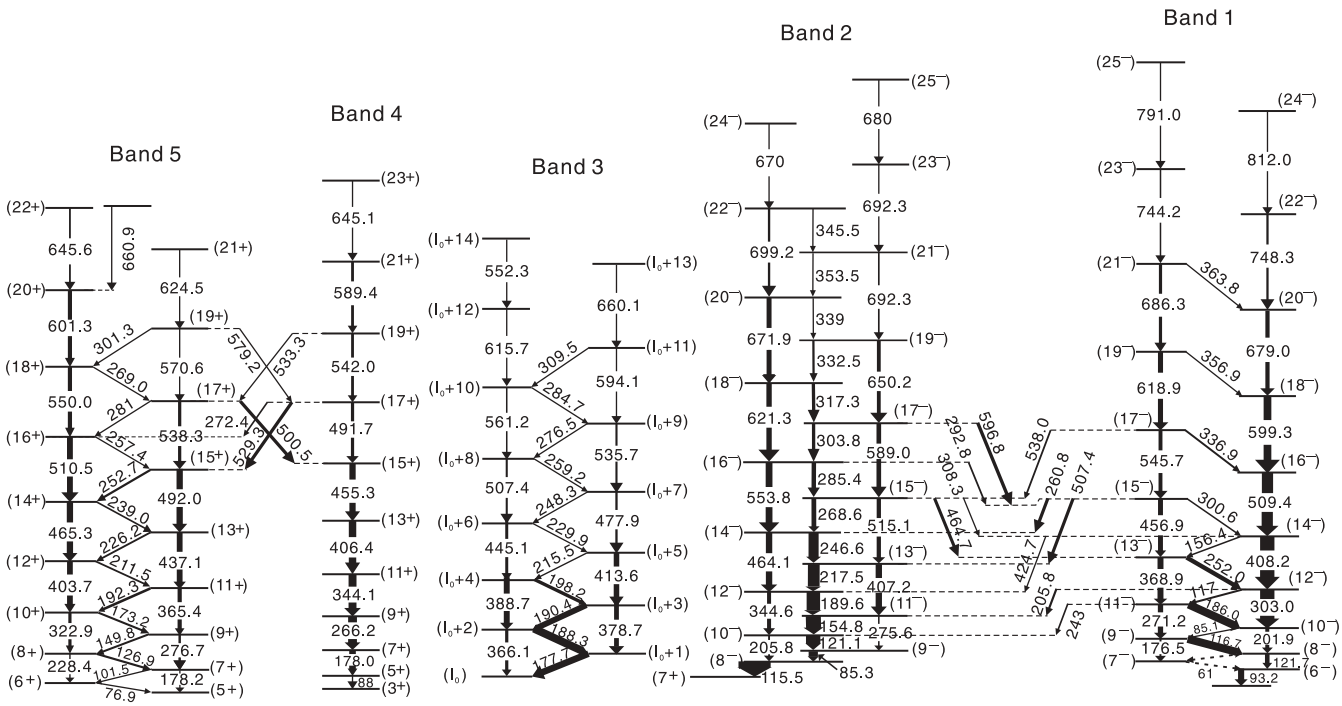

FIG. 3. Level scheme of ^{174}Re deduced from the present work. The widths of the arrows indicate the relative transition intensities.

TABLE I. γ-ray transition energies, initial and final energies of the transitions, spin and parity assignments, relative γ-ray intensities, branching ratios, DCO ratios, ADO ratios, and $B(M1)/B(E2)$ values in ^{174}Re. The transitions are ordered by bands.

E_γ (keV)[a]	$J_i^\pi \rightarrow J_f^\pi$[b]	I_γ[c]	λ[d]	$R_{\rm DCO}$	$R_{\rm ADO}$	$B(M1)/B(E2)$[e]
Band 1						
93.2	$(6^-) \rightarrow$	37		0.76(8)	0.94(19)	
121.7	$(8^-) \rightarrow (6^-)$	27.7		0.83(24)	1.12(18)	
176.5	$(9^-) \rightarrow (7^-)$	12			1.10(46)	
116.7	$(9^-) \rightarrow (8^-)$	48	0.12(3)		0.63(12)	0.63(16)
201.9	$(10^-) \rightarrow (8^-)$	24.9		0.97(11)	1.20(21)	
85.1	$(10^-) \rightarrow (9^-)$	7.4	0.99(12)	0.51(15)	0.71(18)	0.39(5)
271.2	$(11^-) \rightarrow (9^-)$	32		0.93(10)	1.10(18)	
186.0	$(11^-) \rightarrow (10^-)$	48.5	0.73(7)	0.45(5)	0.56(8)	0.21(2)
303.0	$(12^-) \rightarrow (10^-)$	86.7		0.93(9)	1.17(10)	
117	$(12^-) \rightarrow (11^-)$	12.1				
368.9	$(13^-) \rightarrow (11^-)$	36		1.16(21)	1.09(20)	
252.0	$(13^-) \rightarrow (12^-)$	26.6	1.27(12)	0.54(6)	0.59(12)	0.23(2)
408.2	$(14^-) \rightarrow (12^-)$	86.7		0.87(8)	1.18(16)	
156.4	$(14^-) \rightarrow (13^-)$	9.3	13.8(2.2)		0.57(21)	0.15(3)
456.9	$(15^-) \rightarrow (13^-)$	29.8		0.94(22)	1.17(17)	
300.6	$(15^-) \rightarrow (14^-)$	9.3	1.69(22)	0.33(3)	0.48(10)	0.30(4)
509.4	$(16^-) \rightarrow (14^-)$	67.9		0.90(10)	1.18(16)	
545.7	$(17^-) \rightarrow (15^-)$	23.6		1.09(19)	1.17(48)	
336.9	$(17^-) \rightarrow (16^-)$	11.8	2.4(3)	0.46(18)	0.61(13)	0.36(4)
599.3	$(18^-) \rightarrow (16^-)$	46.7		0.88(16)	1.22(26)	
618.9	$(19^-) \rightarrow (17^-)$	30.7		0.86(23)	1.08(27)	
356.9	$(19^-) \rightarrow (18^-)$	$\leqslant 8$	3.2(10)		0.61(15)	0.43(14)
679.0	$(20^-) \rightarrow (18^-)$	25.5		1.00(17)	1.22(25)	
686.3	$(21^-) \rightarrow (19^-)$	19.3		1.31(36)	1.40(33)	
363.8	$(21^-) \rightarrow (20^-)$	$\leqslant 8$				
748.3	$(22^-) \rightarrow (20^-)$	13.7		1.15(28)	1.25(41)	

TABLE I. (*Continued*.)

E_γ (keV)[a]	$J_i^\pi \rightarrow J_f^\pi$[b]	I_γ[c]	λ[d]	R_{DCO}	R_{ADO}	$B(M1)/B(E2)$[e]
744.2	$(23^-) \rightarrow (21^-)$	9.2			1.14(52)	
812.0	$(24^-) \rightarrow (22^-)$	$\leqslant 8$				
791.0	$(25^-) \rightarrow (23^-)$	$\leqslant 8$				
Band 2						
85.3	$(9^-) \rightarrow (8^-)$	28		0.66(22)	0.72(3)	
205.8	$(10^-) \rightarrow (8^-)$	13.2			1.07(13)	
121.1	$(10^-) \rightarrow (9^-)$	87	0.04(1)	0.68(11)	0.89(10)	3.6(5)
275.6	$(11^-) \rightarrow (9^-)$	9.3			1.23(26)	
154.8	$(11^-) \rightarrow (10^-)$	91	0.15(2)	0.69(11)	0.93(9)	1.9(2)
344.6	$(12^-) \rightarrow (10^-)$	24.3		0.98(28)	1.06(18)	
189.6	$(12^-) \rightarrow (11^-)$	100	0.26(2)	0.80(12)	0.93(9)	1.9(2)
407.2	$(13^-) \rightarrow (11^-)$	38.3		1.09(35)	1.26(14)	
217.5	$(13^-) \rightarrow (12^-)$	71	0.46(4)	0.75(11)	0.97(9)	1.64(15)
464.1	$(14^-) \rightarrow (12^-)$	38.6		1.27(23)	1.20(15)	
246.6	$(14^-) \rightarrow (13^-)$	61.2	0.64(6)	0.88(10)	0.95(9)	1.55(14)
515.1	$(15^-) \rightarrow (13^-)$	25.8		0.80(23)	1.08(13)	
268.6	$(15^-) \rightarrow (14^-)$	28.7	0.83(9)	0.81(17)	0.98(12)	1.6(2)
553.8	$(16^-) \rightarrow (14^-)$	41.1		1.20(20)	1.16(22)	
285.4	$(16^-) \rightarrow (15^-)$	26.9	2.1(3)	0.94(25)	0.90(18)	0.76(9)
589.0	$(17^-) \rightarrow (15^-)$	28		0.71(10)	1.05(13)	
303.8	$(17^-) \rightarrow (16^-)$	20	0.80(9)	0.84(16)	0.84(14)	2.2(2)
621.3	$(18^-) \rightarrow (16^-)$	32.4		1.25(22)	1.22(39)	
317.3	$(18^-) \rightarrow (17^-)$	20.1	1.7(2)	0.59(14)	0.97(30)	1.17(13)
650.2	$(19^-) \rightarrow (17^-)$	23		0.95(23)	1.33(35)	
332.5	$(19^-) \rightarrow (18^-)$	13.7	2.6(6)	1.17(36)	1.12(24)	0.86(20)
671.9	$(20^-) \rightarrow (18^-)$	30		1.00(34)	1.03(26)	
339	$(20^-) \rightarrow (19^-)$	$\leqslant 8$	4.5(2.1)	0.76(34)	0.90(44)	0.54(26)
692.3	$(21^-) \rightarrow (19^-)$	$\leqslant 8$				
353.5	$(21^-) \rightarrow (20^-)$	$\leqslant 8$			0.88(26)	
699.2	$(22^-) \rightarrow (20^-)$	14.1		0.77(34)	0.85(30)	
345.5	$(22^-) \rightarrow (21^-)$	$\leqslant 8$			0.70(23)	
692.3	$(23^-) \rightarrow (21^-)$	$\leqslant 8$				
670	$(24^-) \rightarrow (22^-)$	$\leqslant 8$				
680	$(25^-) \rightarrow (23^-)$	$\leqslant 8$				
Transitions	from 1 to 2					
243	$(11^-) \rightarrow (10^-)$	10			0.93(18)	
205.8	$(12^-) \rightarrow (11^-)$	13.2			1.20(34)	
424.7	$(14^-) \rightarrow (12^-)$	7.7			0.82(28)	
507.4	$(15^-) \rightarrow (13^-)$	19.1		1.37(42)	1.28(18)	
260.8	$(15^-) \rightarrow (14^-)$	19.5		0.83(18)	0.90(15)	
538.0	$(17^-) \rightarrow (15^-)$	11		1.20(38)	1.07(38)	
Transitions	from 2 to 1					
464.7	$(15^-) \rightarrow (13^-)$	18.7		1.02(28)	1.20(15)	
308.3	$(15^-) \rightarrow (14^-)$	$\leqslant 8$		0.49(9)	0.48(15)	
292.8	$(16^-) \rightarrow (15^-)$	10.8		1.42(51)	0.72(43)	
596.8	$(17^-) \rightarrow (15^-)$	20.5		1.17(54)	1.06(62)	
Transitions	from 2					
115.5	$(8^-) \rightarrow (7^+)$	194.7		0.53(9)	0.75(7)	
Band 3						
177.7	$(I_0+1) \rightarrow (I_0)$	$\geqslant 40$		1.00(11)	1.11(10)	
366.1	$(I_0+2) \rightarrow (I_0)$	22.1		1.24(33)	1.46(46)	
188.3	$(I_0+2) \rightarrow (I_0+1)$	55	0.45(5)	1.06(27)	1.17(15)	1.5(2)
378.7	$(I_0+3) \rightarrow (I_0+1)$	29		1.13(22)	1.22(31)	
190.4	$(I_0+3) \rightarrow (I_0+2)$	35.3	0.80(8)	0.94(27)	1.21(10)	0.98(10)
388.7	$(I_0+4) \rightarrow (I_0+2)$	25.5		1.06(23)	1.31(25)	
198.2	$(I_0+4) \rightarrow (I_0+3)$	20.7	1.63(16)	1.05(19)	1.15(10)	0.48(5)
413.6	$(I_0+5) \rightarrow (I_0+3)$	33.4		1.01(15)	1.28(20)	
215.5	$(I_0+5) \rightarrow (I_0+4)$	8.4	2.9(2)	0.89(14)	1.00(18)	0.29(2)

TABLE I. (*Continued.*)

E_γ (keV)[a]	$J_i^\pi \rightarrow J_f^\pi$[b]	I_γ[c]	λ[d]	$R_{\rm DCO}$	$R_{\rm ADO}$	$B(M1)/B(E2)$[e]
445.1	$(I_0+6) \rightarrow (I_0+4)$	18		0.91(8)	1.21(17)	
229.9	$(I_0+6) \rightarrow (I_0+5)$	4.5	3.9(3)	0.88(27)	1.01(19)	0.25(2)
477.9	$(I_0+7) \rightarrow (I_0+5)$	13.9		0.92(13)	1.08(17)	
248.3	$(I_0+7) \rightarrow (I_0+6)$	$\leqslant 8$	8.3(1.2)	0.99(25)	1.09(22)	0.13(2)
507.4	$(I_0+8) \rightarrow (I_0+6)$	12.5		1.10(30)	1.24(22)	
259.2	$(I_0+8) \rightarrow (I_0+7)$	$\leqslant 8$	9.2(1.5)	0.72(17)	1.05(30)	0.14(2)
535.7	$(I_0+9) \rightarrow (I_0+7)$	12.8		0.97(19)	1.00(14)	
276.5	$(I_0+9) \rightarrow (I_0+8)$	$\leqslant 8$	8.3(1.2)	1.35(28)	1.41(51)	0.17(2)
561.2	$(I_0+10) \rightarrow (I_0+8)$	9.2		1.08(20)	1.21(21)	
284.7	$(I_0+10) \rightarrow (I_0+9)$	$\leqslant 8$				
594.1	$(I_0+11) \rightarrow (I_0+9)$	$\leqslant 8$			1.19(31)	
309.5	$(I_0+11) \rightarrow (I_0+10)$	$\leqslant 8$				
615.7	$(I_0+12) \rightarrow (I_0+10)$	$\leqslant 8$			1.06(32)	
660.1	$(I_0+13) \rightarrow (I_0+11)$	$\leqslant 8$				
552.3	$(I_0+14) \rightarrow (I_0+12)$	$\leqslant 8$				
Band 4						
88	$(5^+) \rightarrow (3^+)$	$\leqslant 8$				
178.0	$(7^+) \rightarrow (5^+)$	$\geqslant 40$		0.94(10)	1.18(12)	
266.2	$(9^+) \rightarrow (7^+)$	53.3		0.99(9)	1.14(21)	
344.1	$(11^+) \rightarrow (9^+)$	48		0.82(9)	1.18(14)	
406.4	$(13^+) \rightarrow (11^+)$	45		0.98(10)	1.28(17)	
455.3	$(15^+) \rightarrow (13^+)$	37.9		1.01(10)	1.12(13)	
491.7	$(17^+) \rightarrow (15^+)$	19.4		1.12(15)	1.18(16)	
542.0	$(19^+) \rightarrow (17^+)$	17		0.89(11)	1.17(14)	
589.4	$(21^+) \rightarrow (19^+)$	17		0.84(13)	1.34(34)	
645.1	$(23^+) \rightarrow (21^+)$	6.6				
Band 5						
76.9	$(6^+) \rightarrow (5^+)$	$\leqslant 8$				
178.2	$(7^+) \rightarrow (5^+)$	$\leqslant 8$		0.79(38)	0.87(40)	
101.5	$(7^+) \rightarrow (6^+)$	$\leqslant 8$	0.70(18)	0.41(7)	0.46(14)	0.17(4)
228.4	$(8^+) \rightarrow (6^+)$	8.6		0.77(12)	1.06(18)	
126.9	$(8^+) \rightarrow (7^+)$	13	0.72(9)	0.63(9)	0.68(16)	0.29(3)
276.7	$(9^+) \rightarrow (7^+)$	12.7		0.93(17)	1.12(26)	
149.8	$(9^+) \rightarrow (8^+)$	12.3	0.97(9)	0.50(8)	0.64(14)	0.34(3)
322.9	$(10^+) \rightarrow (8^+)$	19.3		1.15(19)	1.15(20)	
173.2	$(10^+) \rightarrow (9^+)$	12.6	1.5(2)	0.51(7)	0.71(12)	0.32(4)
365.4	$(11^+) \rightarrow (9^+)$	25.3		0.85(11)	1.17(22)	
192.3	$(11^+) \rightarrow (10^+)$	15.8	2.4(3)	0.45(8)	0.58(11)	0.27(3)
403.7	$(12^+) \rightarrow (10^+)$	34.8		1.08(13)	1.24(17)	
211.5	$(12^+) \rightarrow (11^+)$	10.9	3.5(4)	0.43(8)	0.63(11)	0.22(2)
437.1	$(13^+) \rightarrow (11^+)$	35		0.96(11)	1.18(11)	
226.2	$(13^+) \rightarrow (12^+)$	11.4	2.9(2)	0.45(6)	0.56(11)	0.33(3)
465.3	$(14^+) \rightarrow (12^+)$	38		1.08(12)	1.11(14)	
239.0	$(14^+) \rightarrow (13^+)$	10.1	3.3(5)	0.49(10)	0.71(14)	0.34(5)
492.0	$(15^+) \rightarrow (13^+)$	38		0.91(14)	1.11(20)	
252.7	$(15^+) \rightarrow (14^+)$	13.5	5.2(1.4)	0.56(8)	0.69(14)	0.24(6)
510.5	$(16^+) \rightarrow (14^+)$	35.4		0.97(12)	1.16(22)	
257.4	$(16^+) \rightarrow (15^+)$	$\leqslant 8$	6.6(1.2)	0.38(11)	0.69(28)	0.21(4)
538.3	$(17^+) \rightarrow (15^+)$	19.5		1.35(39)	1.49(26)	
281.0	$(17^+) \rightarrow (16^+)$	$\leqslant 8$				
550.0	$(18^+) \rightarrow (16^+)$	25.2		0.98(17)	1.45(24)	
269.0	$(18^+) \rightarrow (17^+)$	$\leqslant 8$			0.71(20)	
570.6	$(19^+) \rightarrow (17^+)$	8			1.07(31)	
301.3	$(19^+) \rightarrow (18^+)$	$\leqslant 8$				
601.3	$(20^+) \rightarrow (18^+)$	25		0.94(15)	1.19(27)	
624.5	$(21^+) \rightarrow (19^+)$	8				
645.6	$(22^+) \rightarrow (20^+)$	10.8		0.74(30)	0.99(44)	

TABLE I. (*Continued*.)

E_γ (keV)[a]	$J_i^\pi \rightarrow J_f^\pi$[b]	I_γ[c]	λ[d]	R_{DCO}	R_{ADO}	$B(M1)/B(E2)$[e]
Transitions	from 4 to 5					
529.3	$(17^+) \rightarrow (15^+)$	19.8		1.11(24)	1.35(24)	
272.4	$(17^+) \rightarrow (16^+)$	$\leqslant 8$				
533.3	$(19^+) \rightarrow (17^+)$	8			1.05(25)	
Transitions	from 5 to 4					
500.5	$(17^+) \rightarrow (15^+)$	19.9		1.04(13)	1.14(18)	
579.2	$(19^+) \rightarrow (17^+)$	4.3		0.81(29)	0.96(18)	
Transitions	to 5					
660.9	$() \rightarrow (20^+)$	$\leqslant 5$		0.65(23)	0.97(39)	

[a]Uncertainties between 0.1 and 0.5 keV.
[b]See text for details about the spin and parity assignments.
[c]Uncertainties between 5 and 30%.
[d]Branching ratio: $T_\gamma(I \rightarrow I-2)/T_\gamma(I \rightarrow I-1)$, $T_\gamma(I \rightarrow I-2)$, and $T_\gamma(I \rightarrow I-1)$ are the relative γ intensities of the $E2$ and $M1$ transitions depopulating the level I, respectively.
[e]Extracted from the branching ratios assuming $\delta = 0$.

Fig. 3. However, the larger experimental internal conversion coefficient value relative to the theoretical can probably be attributed to the fact that the bandhead of band 2 has a rather long lifetime that results in a portion of the 115.5-keV transition exceeding the time window. Similar isomeric states have been observed in ^{176}Re [4] and ^{176}Ir [30]. The isomeric lifetime can be roughly estimated by using the experimental internal conversion coefficient 0.62, the theoretical internal conversion coefficient 0.27, and the time window of 200 ns: $T_{1/2} = 200/\log_{1/2}^{(1-\frac{1+0.27}{1+0.62})} = 91$ ns. Gamma rays linking bands 1 and 2 could be established from the gated coincidence spectrum of Fig. 4(c), combined with those of Figs. 4(a) and 4(b). These connections fix unambiguously the spins and parity of one band relative to the other.

Figures 5, 6(a), and 6(b) present the respective coincidence spectra for the newly constructed bands 3 and 5, as well as for band 4. Concerning band 4, the previously known sequence with a topmost level with a suggested spin and parity (19^+) has been extended to a (23^+) state. The transitions which link band 5 to band 4 presumably come from the mixing caused by the near degeneracy of pairs of levels at 15-19 $\hbar$. The transitions linking bands 4 and 5 are visible in Fig. 6(c). Again, the connections unambiguously fix the relative spins and parity of these two bands.

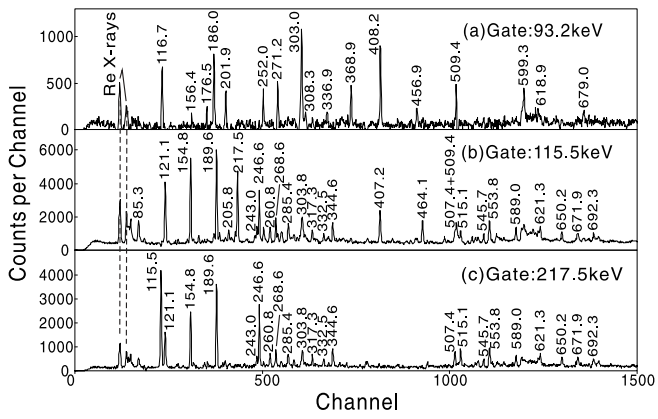

FIG. 4. Representative coincidence spectra gated by the (a) 93.2-, (b) 115.5-, and (c) 217.5-keV transitions in bands 1 and 2, showing the in-band as well as the interband transitions between them.

III. DISCUSSION

A. Preliminary remarks

Nuclei in the vicinity of ^{174}Re are expected to be prolate deformed with a quadrupole deformation parameter $\beta \approx 0.2$. The neutron $\nu 1/2^-[521]$, $\nu 5/2^-[512]$, $\nu 7/2^+[633]$ orbitals and the proton $\pi 1/2^-[541]$, $\pi 9/2^-[514]$, $\pi 5/2^+[502]$ orbitals come very close to their respective Fermi levels. As shown in Fig. 7, such active one-quasiparticle bands have been systematically observed in this mass region.

A first approximation to the excitation spectra of deformed odd-odd nuclei is derived from the coupling of the quasiproton and quasineutron by consulting the associated single-particle energies of neighboring odd-mass nuclei. This coupling is normally additive for the excitation energy as well as for the projection quantum number K:

$$E_K = E_p + E_n, \tag{4}$$

$$K = |\Omega_p \pm \Omega_n|. \tag{5}$$

The results are listed in Table II.

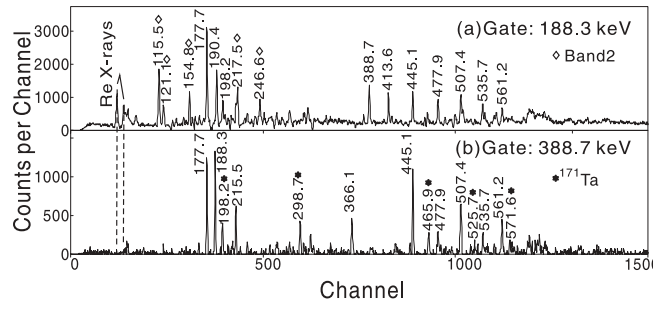

FIG. 5. Representative coincidence spectra gated by the (a) 188.3- and (b) 388.7-keV transitions in band 3. The contamination from band 2 in (a) is in coincidence with the 189.6-keV transition. The absence of Re K x rays in (b) is the result of the subtraction of background in order to suppress the contamination from ^{171}Ta.

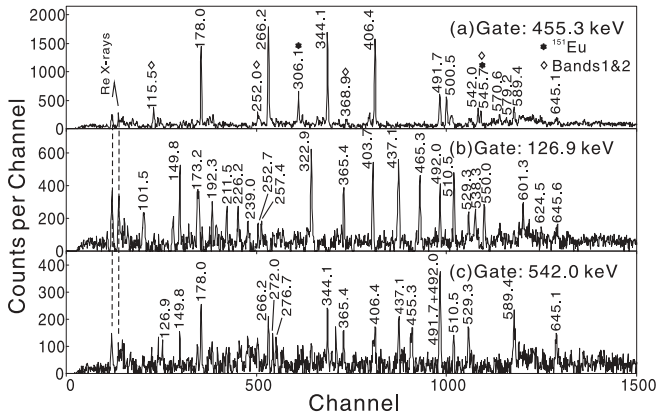

FIG. 6. Representative coincidence spectra gated by the (a) 455.3-, (b) 126.9-, and (c) 542.0-keV transitions in bands 4 and 5, showing in-band as well as interband transitions.

The degeneracy of the two bands with $K = \Omega_p \pm \Omega_n$ can be broken by the proton-neutron (p-n) residual interaction. According to the Gallagher-Moszkowski coupling rules [31], the spin-parallel band is lower in energy than its spin-antiparallel counterpart, which is distinguished by the quantum number of the spin projection Σ. Here, $\Sigma = 1$ (0) denotes the spin-parallel (spin-antiparallel) band. As for the $K = 0$ bands, the p-n residual interaction will further result in the so-called Newby shift (B_N): the shift of odd- and even-spin rotational levels relative to each other. Therefore, the two-quasiparticle excitation energy can be calculated as the sum of the two odd-nucleon excitations plus terms for the rotational energy and the residual interaction:

$$E_K = E_p + E_n + \frac{\hbar^2}{2\Im}\left[K + (-1)^{K+1} a_p a_n \delta_{K,0}\delta_{\Omega_p,1/2}\delta_{\Omega_n,1/2}\right] - (1/2 - \delta_{\Sigma,0})\Delta E_{\rm GM} + \delta_{K,0}(-1)^I B_N, \quad (6)$$

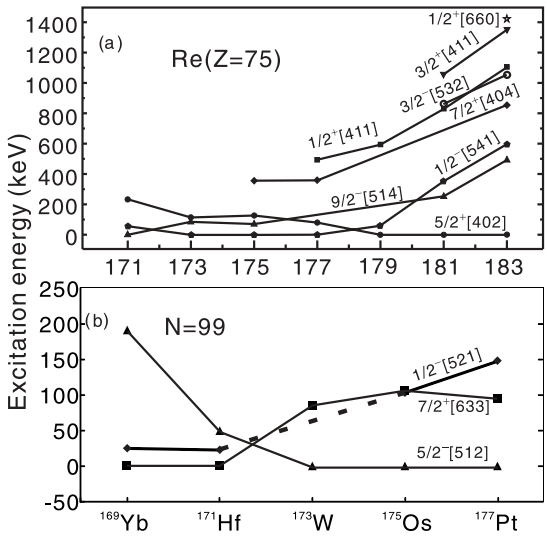

FIG. 7. Bandhead excitation energies for (a) isotopes and (b) isotones of ^{174}Re. The experimental bandhead energies are taken from Refs. [20,21,32–38].

TABLE II. Zero-order level scheme of ^{174}Re. Entries are $K_\pm = |\Omega_p \pm \Omega_n|$ values, zero-order energies in keV, the sign of δ values, and $\Delta E_{\rm GM}$ values. Excitation energies correspond to the average of ^{173}Re and ^{175}Re for protons and to the average of ^{173}W and ^{175}Os for neutrons (the values corresponding to proton and neutron spin-parallel configurations are underlined). The sign of δ values are estimated using Eqs. (13) and (14). $\Delta E_{\rm GM}$ values are extracted from the same configurations listed in Ref. [39].

	$\nu 1/2^-[521]$ 82	$\nu 5/2^-[512]$ 0	$\nu 7/2^+[633]$ 95.5
$\pi 1/2^-[541]$ 0	0^+, $\underline{1^+}$ 82 $-$ $\Delta E_{\rm GM} = 123$	$\underline{2^+}$, 3^+ 0 $\delta < 0$ $\Delta E_{\rm GM} = 136$	$\underline{3^-}$, 4^- 95.5 $\delta < 0$ $\Delta E_{\rm GM} = 144$
$\pi 9/2^-[514]$ 76.4	$\underline{4^+}$, 5^+ 158.4 $\delta > 0$ $\Delta E_{\rm GM} = 60$	2^+, $\underline{7^+}$ 76.4 $\delta > 0$ $\Delta E_{\rm GM} = 104$	1^-, $\underline{8^-}$ 171.9 $\delta > 0$ $\Delta E_{\rm GM} = 60$
$\pi 5/2^+[402]$ 121.7	$\underline{2^-}$, 3^- 203.7 $\delta > 0$ $\Delta E_{\rm GM} = 147$	0^-, $\underline{5^-}$ 121.7 $\delta > 0$ $\Delta E_{\rm GM} = 97$	1^+, $\underline{6^+}$ 217.2 $\delta > 0$ $\Delta E_{\rm GM} = 86$

where a_p (a_n) is the decoupling parameter of the proton (neutron) configuration and $\Im$ the effective moment of inertia with respect to the rotation axis. The results are given in Fig. 8.

The next step is then the extraction of alignments, $B(M1)/B(E2)$ ratios, mixing ratios (δ), and effective K quantum numbers. This is helpful to explain the configuration of the various bands. According to the standard cranked shell model, the quasiparticle alignment can be expressed as

$$i_x(\omega) = I_x(\omega) - R(\omega), \quad (7)$$

where $I_x(\omega)$ is the total aligned angular momentum along the rotation axis and $R(\omega)$ is the collective contribution. The values of $I_x(\omega)$ and ω can be extracted from the level spin I and the experimental level spacings

$$I_x(\omega) = \sqrt{(I+1/2)^2 - K^2}, \quad (8)$$

$$\hbar\omega = \frac{dE(I)}{dI_x(I)} \approx \frac{E(I+1) - E(I-1)}{I_x(I+1) - I_x(I-1)}. \quad (9)$$

The collective component is parametrized using the Harris expression

$$R_x(\omega) = J_0\omega + J_1\omega^3. \quad (10)$$

Starting from Eqs. (7)–(10), we plot the observed aligned angular momenta for the bands in ^{174}Re in Fig. 9, using individual references which give relatively constant aligned angular momenta before a band crossing occurs (see Table III). For the purpose of comparison, we also provide the alignments of neighboring nuclei.

The comparison of experimental $B(M1)/B(E2)$ values with theoretical ones is exhibited in Fig. 10. Theoretical $B(M1)/B(E2)$ ratios have been estimated using the

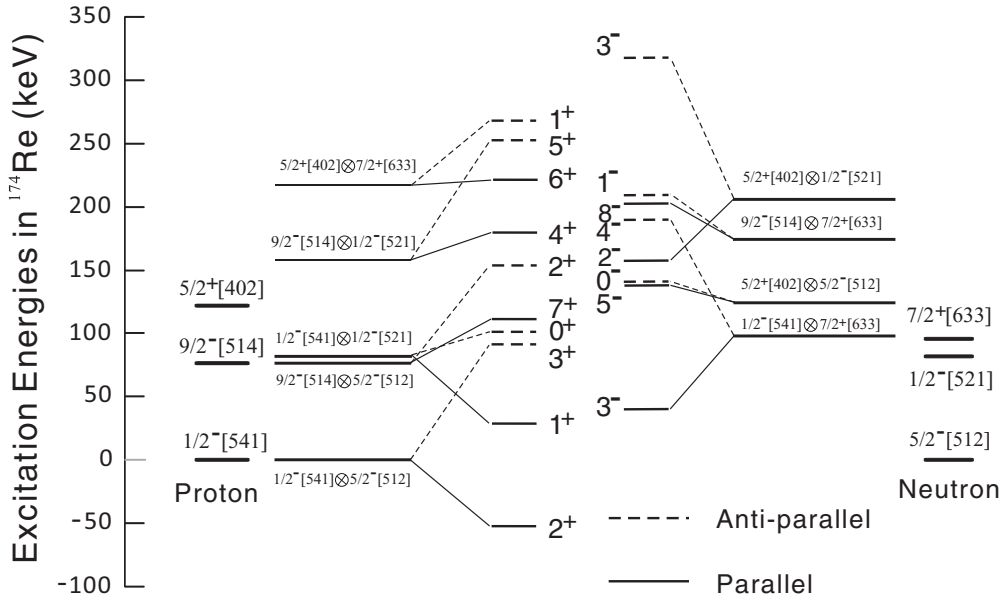

FIG. 8. Estimated two-quasiparticle excitation energies in ^{174}Re. The experimental bandhead energies extracted from neighboring odd-A nuclei; the zero-order level scheme obtained by adding them, respectively; and the estimated excitation energies taking into account the GM splitting and B_N shifts are shown. See text for details.

semiclassical formula developed by Donau and Frauendorf [40]:

$$B(M1, I \to I-1) = \frac{3}{8\pi}\mu_T^2 \tag{11}$$

and

$$B(E2, I \to I-2) = \frac{5}{16\pi}\langle IK20|I-2K\rangle^2 Q_0^2, \tag{12}$$

where the transverse magnetic moment μ_T in units of μ_N is given by

$$\mu_T = \left(g_{\Omega_p} - g_R\right)\left(\Omega_p\sqrt{1-K^2/I^2} - i_p K/I\right) + \left(g_{\Omega_n} - g_R\right)\left(\Omega_n\sqrt{1-K^2/I^2} - i_n K/I\right). \tag{13}$$

Here g_{Ω_p} and g_{Ω_n} are the proton and neutron gyromagnetic factors, respectively. The quantities i_p and i_n represent the aligned angular momenta of the proton and the neutron, respectively. These values are taken from the compilation in Refs. [4,44] and can be found in Table III. Concerning the quadrupole moment, we refer to $Q_0 = 7.3\,eb$ of the ground-state band in ^{172}W [45]. A common collective gyromagnetic factor $g_R = 0.3$ was used in the calculations.

The mixing ratio δ for $\Delta I = 1$ in-band transitions was evaluated using the expression

$$\delta = 0.93 E_\gamma Q_0 K\sqrt{I^2 - K^2}/(\mu_T I^2), \tag{14}$$

TABLE III. Parameters used in the calculations of $B(M1)/B(E2)$ ratios and alignments i_x in the five bands in ^{174}Re and the associated nuclei [41–43]. See text for details.

Nucleus	Band	K^π	$J_0/\hbar^2$ (MeV^{-1})	$J_1/\hbar^4$ (MeV^{-3})	i_x ($\hbar$)	g_Ω (MeV)
^{172}W	gsb	0^+	24	255		
^{174}W	gsb	0^+	27	157		
^{173}Re	$1/2^-[541](h_{9/2})$	$1/2^-$	33	45	2.5	0.84
^{173}Re	$9/2^-[514](h_{11/2})$	$9/2^-$	26	72	1.0	1.29
^{173}Re	$5/2^+[402](d_{5/2})$	$5/2^+$	30	432	0.1	1.57
^{173}W	$1/2^-[521]$	$1/2^-$	34	369	0.4	0.71
^{173}W	$5/2^-[512]$	$5/2^-$	29	269	0.6	−0.31
^{173}W	$7/2^+[633](i_{13/2})\ \alpha = 0.5$	$7/2^+$	32	90	2.9	−0.25
^{173}W	$7/2^+[633](i_{13/2})\ \alpha = -0.5$	$7/2^+$	34	75	3.4	−0.25
^{174}Re	Band 1 $\alpha = 1$	3^-	36	70	5.3	
^{174}Re	Band 1 $\alpha = 0$	3^-	33	60	6.1	
^{174}Re	Band 2	8^-	35	110	3.8	
^{174}Re	Band 4	1^+	40	115	2.9	
^{174}Re	Band 5	2^+	34	160	3.3	

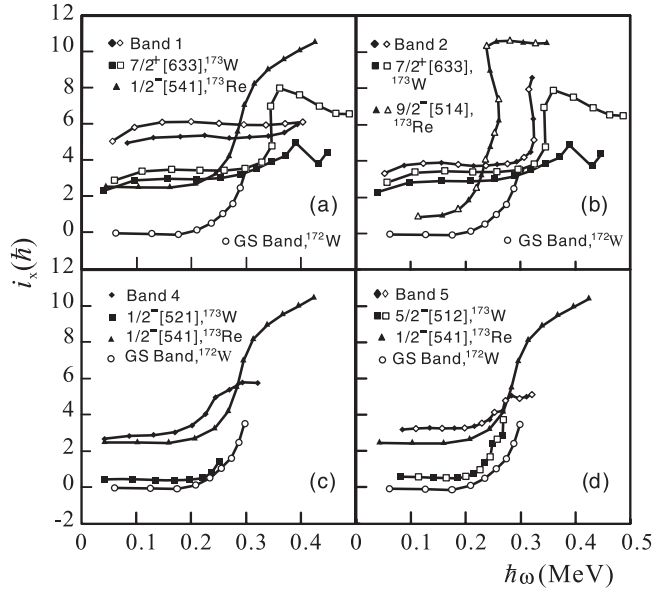

FIG. 9. Experimental alignments as a function of the rotational frequency for (a) band 1, (b) band 2, (c) band 4, and (d) band 5 in ^{174}Re. The Harris parameters are listed in Table III.

where E_γ is the transition energy in MeV. The effective projection quantum number $K_{\rm eff}$ could be deduced from these two expressions [46]:

$$K_1 = (2 - x_1)/(x_1 - 1), \quad K_2 = (7 - 3x_2)/2(x_2 - 1), \quad (15)$$

where the ratio x stands for the first two consecutive transition energies. K_1 is used and x_1 is deduced from the first two $\Delta I = 1$ transitions, when the signature splitting is small; otherwise, one should use K_2 with x_2 deduced from the first two $\Delta I = 2$ transitions instead.

B. Configurations and spin assignments

1. *Band 1*

Band 1 has been reported in our previous publication [16], where the quasiparticle configuration of $\pi h_{9/2}(1/2^-[541]) \otimes \nu i_{13/2}(7/2^+[633])$ was proposed. This assignment was based on the large signature splitting, which is a common feature of semidecoupled bands in this mass region. The much extended band 1 in this work is helpful to extract mixing ratios, $B(M1)/B(E2)$ ratios, and the alignment to check the previously suggested configuration. First, the negative δ ratio, as indicated in Fig. 2(a), is consistent with the suggested configuration (see Table II). This assignment is then further confirmed by the comparison between experimental and calculated $B(M1)/B(E2)$ ratios (see Fig. 10), where the K value is chosen to be 3 with the aid of Gallagher-Moszkowski coupling rules and the estimated excitation energies listed in Fig. 8.

Finally, the large alignment is consistent with the involvement of both the $\pi h_{9/2}$ and $\nu i_{13/2}$ orbitals. In Fig. 9, it is seen that the quasiparticle alignment for band 1 in ^{174}Re is split into two $\Delta I = 2$ branches. Each branch is associated with a signature $\alpha \equiv I(mod2)$. The expected favored signature in

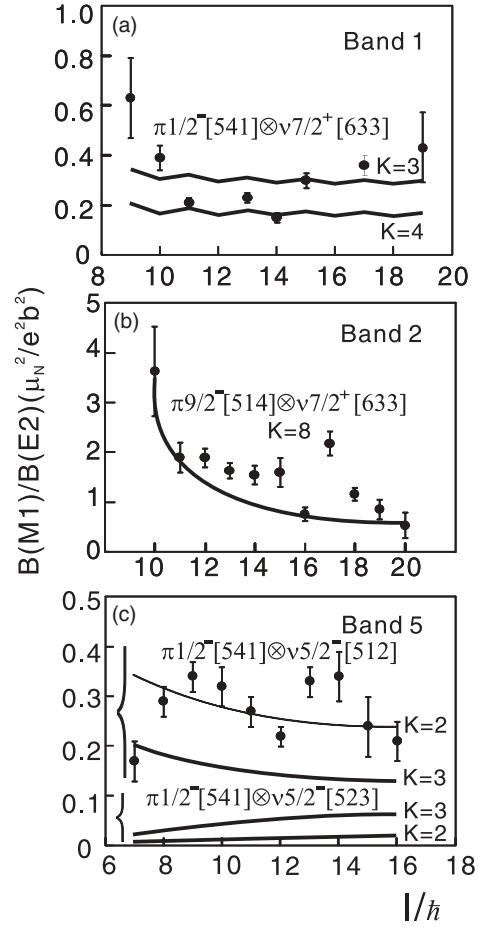

FIG. 10. Experimental $B(M1)/B(E2)$ values corresponding to (a) band 1, (b) band 2, and (c) band 5 in ^{174}Re. The results of the calculations obtained in the framework of the cranked shell model for the configurations relevant to these bands are also shown.

odd-odd nuclei (α^f_{p-n}) corresponds to the coupling between the favored signature of both the proton [$\alpha^f_p = \frac{1}{2}(-1)^{j_p-1/2}$] and the neutron [$\alpha^f_n = \frac{1}{2}(-1)^{j_n-1/2}$] orbitals. For band 1, the initial alignment is around 5.3 $\hbar$ for the favored signature branch ($\alpha^f_{p-n} = 1$) and 5.9 $\hbar$ for the unfavored signature branch ($\alpha^f_{p-n} = 0$). These values are roughly the sum of the individual alignments of the quasiproton (about 2.5 $\hbar$) and the quasineutron (nearly $i = 2.9\hbar$ for the favored branch and $i = 3.4\hbar$ for the unfavored branch) in the corresponding bands in ^{173}W and ^{173}Re. The AB neutron crossing is blocked by a quasineutron occupying the $i_{13/2}$ subshell. Thus, the backbend will correspond to the neutron BC (and AD) crossing taking place at a higher rotational frequency. Since no band crossing was observed up to the highest frequency measured, the band crossing is delayed with respect to the $\nu i_{13/2}$ band in the odd-N neighbor ^{173}W. This can be attributed to the involvement of the $\pi h_{9/2}(1/2^-[541])$ proton. In the rare-earth region, it has been well established that band crossings in the $\pi h_{9/2}(1/2^-[541])$ bands of odd-Z and even-N nuclei are delayed with respect to their even-even neighbors [47,48].

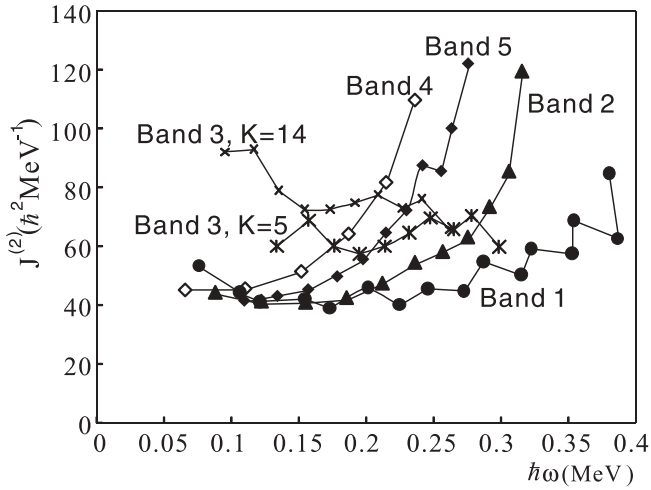

FIG. 11. Dynamical moments of inertia, $J^{(2)}$, as a function of rotational frequency for the five bands in ^{174}Re. $K = 14$ and 5 are used for band 3, corresponding to four-quasiparticle and two-quasiparticle configurations, respectively.

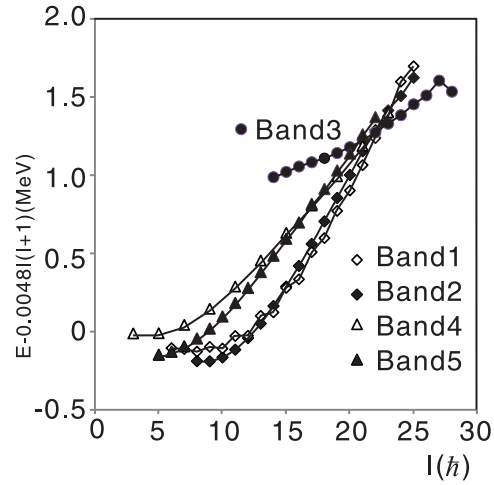

FIG. 12. Excitation energy vs spin for the five rotational bands in ^{174}Re relative to an arbitrary constant rotor.

2. *Band 2*

Band 2 exhibits a strongly coupled character with intense in-band $M1/E2$ transitions and small signature splittings. The strong $M1/E2$ transitions indicate that a high-K and/or a large-g_K factor is involved in this structure. Considering all the possible low-lying negative parity intrinsic states of Fig. 8, we suggest that the configuration $\pi h_{11/2}(9/2^-[514]) \otimes \nu i_{13/2}(7/2^+[633])$ is the best candidate. The experimental DCO ratios indicate positive mixing ratios δ [see Fig. 2(b)], as expected (see Table II). The experimental $B(M1)/B(E2)$ ratios have been deduced and are compared with theoretical calculations in Fig. 10. The agreement is rather good under the assumption of this configuration. Experimental values are slightly higher than theoretical results, which may be due to the neglect of the δ value [0.29 for the $(12^-) \rightarrow (11^-)$ transition]. Two experimental points ($I = 15, 17$) deviate from the trend. This may arise from configuration mixing with band 1 in this spin region.

The alignment of band 2 shown in Fig. 9 follows the additivity rule ($3.8 \approx 1.0 + 2.9\ \hbar$) over a wide range of frequencies. A sharp upbend is observed at $\hbar\omega \approx 0.3$ MeV, but no accurate crossing frequency or alignment gain can be extracted due to the lack of levels after the crossing.

3. *Band 3*

As mentioned in Sec. II, band 3 was assigned to ^{174}Re based on three facts. First, the transitions in band 3 are in coincidence with Re K x rays. Second, the intensities of the transitions in band 3 have a similar trend versus exciting energy as known γ rays in ^{174}Re. Finally, detailed high-spin level schemes for ^{152}Sm, ^{173,175}Re, ^{171}Ta, and ^{174}W helped us to exclude assignments to these other possible reaction channels.

In order to understand the configuration of band 3, we obtain the effective projection quantum number and plot the dynamic moments of inertia (see Fig. 11). The deduced effective projection quantum number $K_{\rm eff} = 15.8$ is too large for a two-quasiparticle configuration. On the other hand, no matter how much the K (such as 5 or 14) is, the dynamic moment of inertia of band 3 is rather large with respect to the above-mentioned two-quasiparticle bands before band crossing. Band 3 is, hence, interpreted as a four-quasiparticle band. Considering the active quasiparticle orbitals, two candidates for a four-quasiparticle band with $K^\pi = 14^-$ are $\pi 9/2^-[514] \otimes \nu 5/2^-[512]$, $7/2^-[514]$, $7/2^+[633]$ and $\pi 9/2^-[514]$, $5/2^+[402]$, $7/2^+[404] \otimes \nu 7/2^+[633]$. For the former, a similar four-quasiparticle band has been identified in ^{180}Re [46,49], with $K_{\rm eff} = 16.96$ and a bandhead energy $E = 1755$ keV. That band was described as $\pi 9/2^-[514] \otimes \nu 5/2^-[512]$, $7/2^-[514]$, $9/2^+[624]$, K^π=15^-. In that case, a large moment of inertia was also obtained and interpreted as the result of reduced pairing and, perhaps, larger deformation. The latter can be regarded as a quasiproton and a quasineutron outside the two-quasiparticle excitation of an even-even core. Such a core excitation $\pi 9/2^-[514] \otimes 7/2^+[404]$, K^π=8^- has been identified in the even-even ^{174}W nucleus [50], with a lifetime of 158(3) ns and an exciting energy of 2268 keV.

Although the bandhead of band 3 has a spin value around 14 and, thus, many possible decay paths to lower-lying structures, no depopulating γ transitions were observed in coincidence, constrained by the experimental time window of 200 ns. Seemingly band 3 has an isomeric bandhead with a half-life larger than 1 μs. To search for the possible cause of the isomeric state, we plotted the excitation energies of all the five bands in ^{174}Re (see Fig. 12). The topmost levels of band 3 should be located near the yrast line, as demonstrated in Fig. 12. Thus the bandhead has an excitation energy of about 2 MeV, which supports the four-quasiparticle assignment. Since this state is about 800 keV higher than the yrast two-quasiparticle states with the same spin, rather small mixtures should be expected between these two families of states, resulting in the existence of the isomeric bandhead.

Furthermore, no strong side feeding was found in the lower-spin region of the other four bands. Because of its hypothetical location high above the yrast line, the decay path of the isomer likely leads to other, unobserved band

structures and is spread out over many different branches. In addition, the lower γ multiplicity of isomer-decay events reduces the coincident detection efficiency further. Thus, the transitions depopulating band 3 are difficult to trace, although the population of band 3 is not weak.

4. Band 4

Due to its unique structural properties, band 4 was interpreted as the favored signature of the $\pi h_{9/2}(1/2^-[541]) \otimes \nu(1/2^-[521])$ doubly decoupled band in our previous work [16]. Because of the large signature splitting, the unfavored $\Delta I = 2$ transition sequence is usually rather difficult to observe. The spacings of level energies and the spins are very similar to those of the ground band of its even-even core ^{172}W. Again, the alignment of band 4 shown in Fig. 9 accounts well for the additivity rule ($2.9\hbar \approx 2.5\hbar + 0.4\hbar$) at lower frequencies below 0.2 MeV. An accurate crossing frequency or an alignment gain can hardly be deduced due to missing level information after the crossing.

5. Band 5

The δ values for the $\Delta I = 1$ intraband transitions in band 5 are negative [see Fig. 2(d)]. As indicated in Table II, the configuration $\pi h_{9/2}(1/2^-[541]) \otimes \nu 5/2^-[512]$ is the only candidate for this band. Experimental and theoretical $B(M1)/B(E2)$ ratios are plotted in Fig. 10. The agreement is satisfactory under the assumption of the $\pi h_{9/2}(1/2^-[541]) \otimes \nu 5/2^-[512]$ quasiparticle configuration with $K = 2$. Since a neutron configuration admixture should occur in band 5, $B(M1)/B(E2)$ ratios for the $\pi h_{9/2}(1/2^-[541]) \otimes \nu 5/2^-[523]$ configuration are also calculated and shown in Fig. 10. It is clear that the agreement with the experimental values is poor compared to the results with the $\pi h_{9/2}(1/2^-[541]) \otimes \nu 5/2^-[512]$ coupling. Thus, the $\nu 5/2^-[512]$ orbital could be the leading parentage in the neutron configuration admixture.

This configuration assignment is also supported by the additivity rule of alignments ($3.3 \approx 2.5 + 0.6\ \hbar$) at lower frequencies below 0.2 MeV (see Fig. 9). Moreover, a band crossing has been observed for band 5 in ^{174}Re at a rotational frequency of about $\hbar\omega \approx 0.25$ MeV, and this is close to the AB band crossing frequency in even-even neighbors.

As band 5 and band 4 are linked in the level scheme, their levels can be compared in energy. The (5^+) state of band 5 is determined to be lower than the (3^+) level of band 4. Thus, the ground state of ^{174}Re should be the intrinsic state of the $1/2^-[541]\otimes 5/2^-[512]$ configuration rather than the $1/2^-[541]\otimes 1/2^-[521]$ configuration.

C. Signature inversion

Typical level staggering curves $S(I) = E(I) - E(I-1) - \frac{1}{2}[E(I+1) - E(I) + E(I-1) - E(I-2)]$ [51] are plotted against I in Figs. 13 and 14. Levels involved in interband transitions are corrected in energy, considering the energy shift caused by level interaction (see Sec. III D). Signature inversion

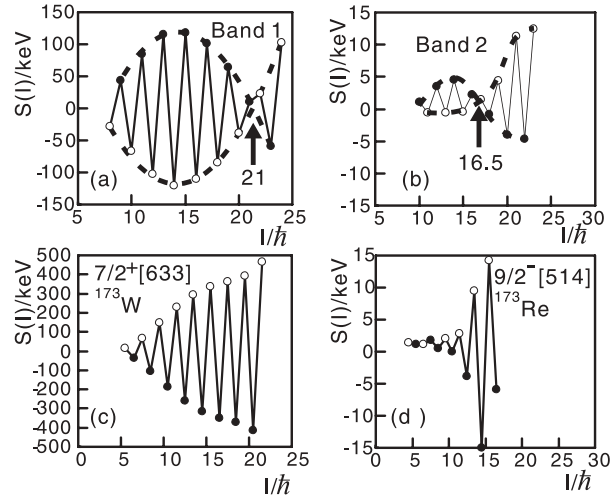

FIG. 13. Plot of signature splitting $S(I)$ vs I for (a) band 1 and (b) band 2 in ^{174}Re and the corresponding one-quasiparticle bands in neighboring (c) ^{173}W and (d) ^{173}Re. The filled (open) symbols correspond to the signature-favored (signature-unfavored) levels. The arrows indicate the spins at which signature crossing occurs.

structures were found in three bands: band 1, band 2, and band 5 with configurations $\pi h_{9/2} \otimes \nu i_{13/2}$, $\pi h_{11/2} \otimes \nu i_{13/2}$, and $\pi h_{9/2} \otimes \nu f_{7/2}$, respectively.

1. Bands 1 and 2

In both configurations, the unfavored branch is lower in energy than the favored one at low spins, where the favored signature corresponds to $\alpha_f = 1$ for the $\pi h_{9/2} \otimes \nu i_{13/2}$ configuration (band 1) and $\alpha_f = 0$ for the $\pi h_{11/2} \otimes \nu i_{13/2}$ state (band 2). With increasing angular momentum, the anomalous signature splitting decreases, and the two signature branches cross each other at $I_c = 21$ for band 1, while $I_c = 16.5$ for band 2. Beyond these spin values, normal signature splitting is restored. These results fit the known systematics well: for the $\pi h_{9/2} \otimes \nu i_{13/2}$ configuration, the spin for signature crossing I_c decreases with decreasing (increasing) two neutrons (protons) [7]; for the $\pi h_{11/2} \otimes \nu i_{13/2}$ configuration, the spin for signature

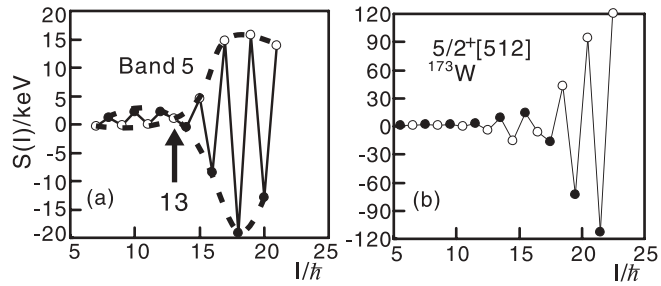

FIG. 14. Plot of signature splitting $S(I)$ vs I for (a) band 5 in ^{174}Re and the corresponding (b) $5/2^-[512]$ band in neighboring ^{173}W. The filled (open) symbols correspond to the signature-favored (signature-unfavored) levels. The arrows indicate the spins at which signature crossing occurs.

crossing I_c increases $2 \sim 3\,\hbar$ with decreasing (increasing) two neutrons (protons), in contrast to the former configuration [6].

The signature splitting amplitude in band 1 is much larger than that in band 2. It is worth noting that the splitting amplitude is mainly determined by the orbital which has a smaller splitting amplitude in the corresponding odd-A nucleus [52]. For band 1 ($\pi h_{9/2}(1/2^-[541]) \otimes \nu i_{13/2}$), it is the $\nu i_{13/2}(7/2^+[633])$ quasineutron rather than the $\pi h_{9/2}(1/2^-[541])$ quasiproton because of its low-Ω and high-j nature, while for band 2 it is the $\pi h_{11/2}(9/2^-[514])$ quasiproton as it has a smaller signature splitting than the $\nu i_{13/2}(7/2^+[633])$ quasineutron. The amplitudes of the $\nu i_{13/2}(7/2^+[633])$ quasineutron and $\pi h_{11/2}(9/2^-[514])$ quasiproton are shown in the lower parts of Fig. 13 for comparison.

2. *Band 5*

Signature splitting in band 5 is slightly reversed in the low-spin region, where the favored (unfavored) signature is signed by $\alpha = 0$ (1). The $\alpha = 1$ branch is lower in energy until the reverse point at $I_c = 13$, beyond which the signature splitting restores to the normal pattern and enlarges soon thereafter. Differing from the two configurations discussed before, the signature inversion in band 5 may be explained by an alternative mechanism, namely, neutron configuration admixture. In the present case, it is the quasineutron that has small signature splitting whereas the $\pi h_{9/2}$ quasiproton contributes only an $\alpha_f = 1/2$ favored signature. Noting that the neutron Fermi surface is located near the close-lying $2f_{7/2}$ and $1h_{9/2}$ subshells, the admixture of states of $2f_{7/2}$ and $1h_{9/2}$ spherical parentages may lead to the low-spin signature inversion observed in band 5. Plots similar to those for the $\nu 1/2^-[521]$ band in ^{173}W [43] (see the right part of Fig. 14) show that the low-spin signature inversion does occur in the one-quasiparticle bands, seemingly providing an argument for this hypothesis.

D. Deformation driving effects by intruder orbitals

The deformation driving effect of an intruder state can be viewed as core polarization originating from a particle occupying a specific intruder orbital, such as the $\pi h_{9/2}(1/2^-[541])$ state. Observed $E2$ linking transitions between the bands involved provides the opportunity to get the ratio of the relative quadrupole moments. In the present work, a series of γ rays linking bands 1 and 2 and five γ rays between bands 4 and 5 (see Fig. 3) have been found in the level scheme of ^{174}Re. This denotes the existence of state mixing between different bands. The interactions can roughly be analyzed within a two-level mixing scheme [53].

Starting from the two unperturbed states $|1\rangle$ and $|2\rangle$, we write the mixed states $|\psi_1\rangle$ and $|\psi_2\rangle$ as

$$|\psi_1\rangle = a|1\rangle + b|2\rangle, \quad |\psi_2\rangle = -b|1\rangle + a|2\rangle, \tag{16}$$

where a and b satisfy the normalization condition $a^2 + b^2 = 1$. The relationship between the interaction matrix element V and the perturbed energies (E_1 and E_2) is then expressed as

$$|V| = ab(E_1 - E_2) = a\sqrt{1 - a^2}(E_1 - E_2). \tag{17}$$

Here these two mixed states are assumed to be de-excited from a pure and unperturbed level ($|\psi_0\rangle$). The coefficients a and b are directly related to the reduced transition possibilities:

$$\frac{B(E2, \psi_0 \to \psi_1)}{B(E2, \psi_0 \to \psi_2)} = \frac{a^2}{b^2}. \tag{18}$$

However, in the cases in ^{174}Re, both initial levels and final levels are mixed. Thus, a more complex formula is employed to solve this problem:

$$\begin{aligned} \frac{B(E2, \psi_{I1} \to \psi_{(I-2)2})}{B(E2, \psi_{I1} \to \psi_{(I-2)1})} &= \left[\frac{a_I b_{I-2} + b_I a_{I-2} Rc}{a_I a_{I-2} + b_I b_{I-2} Rc}\right]^2, \\ \frac{B(E2, \psi_{I2} \to \psi_{(I-2)1})}{B(E2, \psi_{I2} \to \psi_{(I-2)2})} &= \left[\frac{-b_I a_{I-2} + a_I b_{I-2} Rc}{b_I b_{I-2} + a_I a_{I-2} Rc}\right]^2. \end{aligned} \tag{19}$$

Here $R = Q_t(1)/Q_t(2)$ denotes the ratios of intrinsic transition quadrupole moments of the two configurations, and $c = \langle I K_1 20 | I - 2K_1\rangle / \langle I K_2 20 | I - 2K_2\rangle$ is the ratio of Clebsch-Gordan coefficients.

The ratios of reduced transition probabilities are extracted from the experimental data and the results are summarized in Table IV. Note that a and b depend on the interaction strength V. For the sake of simplicity, we neglect the difference of the interaction strength of the initial and final levels. The extracted value of V can, therefore, be regarded as a function of the ratio of the intrinsic transition quadrupole moments R. Then, V-R values can be obtained from the overlap regions (see Fig. 15).

In this way, two V-R functions deduced from the interaction between band 1 and band 2 are demonstrated in Fig. 15(a), from which we can determine $V \approx 3.8$ keV and $R = Q_t(\text{band 2})/Q_t(\text{band 1}) = 0.87 \pm 0.12$. The rather small interaction strength can be understood as being due to the different deformation and K forbiddenness between band 1 ($K = 3$) and band 2 ($K = 8$). For the purpose of comparison with R, total Routhian surface (TRS) calculations were performed to get a deeper understanding of the shape [54–57]. The nonaxial deformed Woods-Saxon potential was employed [58]. Collective rotation is investigated in the frame of the

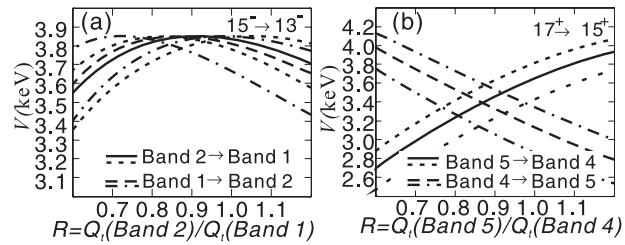

FIG. 15. The interaction strength calculated from the experimental branching ratios plotted as a function of the ratio between the quadrupole moments R: (a) corresponds to bands 1 and 2, while (b) corresponds to bands 4 and 5. For each transition, there are three lines because there is one central value together with the two one-sigma limits.

TABLE IV. The experimentally deduced ratios λ between the γ-ray transition intensities $T_\gamma(E2, I \rightarrow (I-2))$ and the ratios λ_B between the reduced transition probabilities $B(E2, I \rightarrow (I-2))$ for interband and intraband transitions.

Initial level	Interband transition energy	Intraband transition energy	λ	λ_B
Band 4, 17^+	529.3 keV	491.7 keV	0.38 ± 0.09	0.26 ± 0.06
Band 5, 17^+	500.5 keV	538.3 keV	0.36 ± 0.07	0.52 ± 0.10
Band 1, 15^-	507.4 keV	456.9 keV	0.88 ± 0.25	0.52 ± 0.15
Band 2, 15^-	464.7 keV	515.1 keV	2.0 ± 0.5	3.3 ± 0.8

cranked shell model in the three-dimensional deformation spaces of β_2, β_4, and γ. The calculations indicate apparent shape changes below the backbending, and typical TRS plots corresponding to the two bands of interest are shown in Fig. 16. According to the calculations, states of band 1 ($\beta_2 = 0.244$) have a larger quadrupole deformation than the states of band 2 ($\beta_2 = 0.207$). The ratio $\beta_{2\,\text{band}\,2}/\beta_{2\,\text{band}\,1} \approx 0.85$ agrees with the result from the analysis of the experimental interaction strength.

In odd-A rhenium isotopes, the intruder state $1/2^-[541]$ can give rise to apparent deformation driving effects [8]. For example, in the study of ^{177}Re [59], the difference in deformation between the $1/2^-[541]$ and $9/2^-[514]$ orbitals was deduced to be 15%, by means of the recoil distance measurement technique. However, as the $i_{13/2}(7/2^+[633])$ quasineutron is taken into account, the difference in deformation between the $\pi h_{9/2}(1/2^-[541]) \otimes \nu i_{13/2}(7/2^+[633])$ and $\pi h_{11/2}(9/2^-[514]) \otimes \nu i_{13/2}(7/2^+[633])$ configurations is still about 15% in the present work. Thus, seemingly the quasineutron is only a spectator for the driving effect on nuclear deformation.

For the interaction between band 4 ($K = 1$) and band 5 ($K = 2$), the values $V \approx 3.4$ keV, $R = Q_t(\text{band}\,5)/Q_t(\text{band}\,4) = 0.87 \pm 0.10$ are deduced [Fig. 15(b)]. The $1/2^-[521]$ orbital is becoming lower in energy with increasing quadrupole β_2 deformation around $\beta = 0.2$. Thus, it can drive the nuclei to a state with larger deformation, as well. In a previous work on ^{175}Os [10], near degeneracy of rotational states at spin 25/2 and 29/2 in the $1/2^-[521]$ and $5/2^-[512]$ bands was reported and a very small interaction matrix element of about 4 keV was suggested to be due to a 25% difference in deformation between the two configurations. Using the parameters of Ref. [10], a result of $Q_t(1/2^-[521])/Q_t(5/2^-[512]) = 1.09 \pm 0.13$ is calculated. The interaction strength and the difference in deformation deduced in these two bands in ^{174}Re are similar to those in ^{175}Os, indicating that the deformation driving effect contributed by the quasiproton can be omitted.

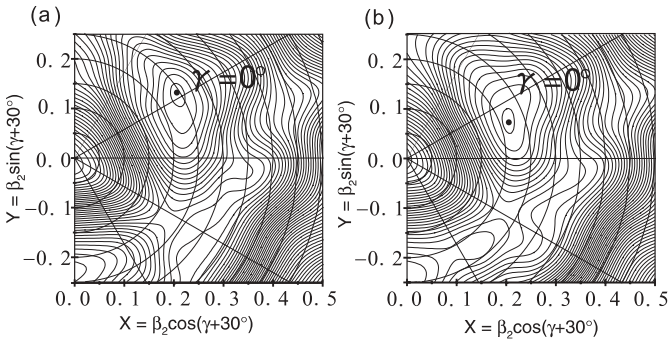

FIG. 16. Total Routhian surface calculations for the (a) band 1 and (b) band 2 configurations of ^{174}Re at a rotational frequency $\hbar\varpi = 0.2$ MeV, corresponding to spin $I \approx 14$. The two minima are at $\beta_2 = 0.244$, $\beta_4 = -0.002$, $\gamma = +2.743^\circ$ and $\beta_2 = 0.207$, $\beta_4 = -0.010$, $\gamma = -10.51^\circ$, respectively.

IV. CONCLUSIONS

In conclusion, high-spin states in odd-odd ^{174}Re have been investigated further with in-beam γ-spectroscopy techniques. Five rotational bands have been observed and their configurations discussed. Apart from the much extended $\pi h_{9/2} \otimes \nu i_{13/2}$, $\pi h_{11/2} \otimes \nu i_{13/2}$, and $\pi h_{9/2} \otimes \nu 1/2^-[521]$ bands, a four-quasiparticle band and a new two-quasiparticle band based on the $\pi 1/2^-[541] \otimes \nu 5/2^-[512]$ configuration have been identified in this work. The four-quasiparticle band should have an isomeric bandhead. A $\pi 1/2^-[541] \otimes \nu 5/2^-[512]$ configuration has been suggested as the intrinsic configuration for the ground state in ^{174}Re. In the $\pi h_{9/2} \otimes \nu i_{13/2}$ and the $\pi h_{11/2} \otimes \nu i_{13/2}$ bands, low-spin signature inversion has been found, consistent with systematics. The $\pi 1/2^-[541] \otimes \nu 5/2^-[512]$ band also exhibits an anomalous signature splitting at low rotational frequencies. Admixture between neutron orbitals has been suggested to explain this slight inversion. Bands 1 and 4 have been deduced to have larger deformation than bands 2 and 5, respectively. These differences in deformation could be attributed to the deformation driving effects by quasiparticles occupying the $\pi 1/2^-[541]$ and $\nu 1/2^-[521]$ states.

ACKNOWLEDGMENTS

The authors wish to thank the staff of the Japan Atomic Energy Agency tandem accelerator for providing the ^{27}Al beam and for their hospitality during the experiment. This work was partially supported by the National Natural Sciences Foundation of China (Grants No. 11175217, No. 10825522, No. 11105186, and No. 10735010), the Major State Basic Research Developing Program of China (Grant No. 2007CB815000), and the Chinese Academy of Sciences.

[1] G. García Bermúdez and M. A. Cardona, Phys. Rev. C **64**, 034311 (2001).

[2] L. L. Riedinger, H. Q. Jin, W. Reviol, J.-Y. Zhang, R. A. Bark, G. B. Hagemann, and P. B. Semmes, Prog. Part. Nucl. Phys. **38**, 251 (1997).

[3] Y. Liu, Y. Ma, H. Yang, and S. Zhou, Phys. Rev. C **52**, 2514 (1995).

[4] M. A. Cardona, A. J. Kreiner, D. Hojman, G. Levinton, M. E. Debray, M. Davidson, J. Davidson, R. Pirchio, H. Somacal, D. R. Napoli, D. Bazzacco, N. Blasi, R. Burch, D. De Acuña, S. M. Lenzi, G. Lo Bianco, J. Rico, and C. R. Alvarez, Phys. Rev. C **59**, 1298 (1999).

[5] Y. H. Zhang, T. Hayakawa, M. Oshima, Y. Toh, J. Katakura, Y. Hatsukawa, M. Matsuda, N. Shinohara, T. Ishii, H. Kusakari, M. Sugawara, and T. Komatsubara, Eur. Phys. J. A **8**, 439 (2000).

[6] Y. Liu, Y. Ma, H. Yang, and S. Zhou, Phys. Rev. C **52**, 2514 (1995).

[7] Y. H. Zhang, M. Oshima, Y. Toh, X. H. Zhou, M. Koizumi, A. Osa, A. Kimura, Y. Hatsukawa, T. Morikawa, M. Nakamura, M. Sugawara, H. Kusakari, T. Komatsubara, K. Furuno, H. L. Wang, P. Luo, C. S. Wu, and F. R. Xu, Phys. Rev. C **68**, 054313 (2003).

[8] R. A. Bark, R. Bengtsson, and H. Carlsson, Phys. Lett. B **339**, 11 (1994).

[9] D. Hojman, M. A. Cardona, D. R. Napoli, S. M. Lenzi, J. Davidson, M. Davidson, C. A. Ur, G. Lo Bianco, C. M. Petrache, M. Axiotis, D. Bazzacco, M. De Poli, G. de Angelis, E. Farnea, T. Kroell, S. Lunardi, N. Marginean, T. Martínez, R. Menegazzo, B. Quintana, and C. Rossi Alvarez, Phys. Rev. C **67**, 024308 (2003).

[10] G. D. Dracoulis and B. Fabricius, Phys. Rev. C **41**, 2933 (1990).

[11] E. E. Berlovich, P. P. Vaishnis, and V. D. Vitman, Iza. Akad. Nauk SSSR(Ser Fiz) **33**, 1705 (1974).

[12] A. Szymanski, G. W. A. Newton, V. J. Robinson, and H. E. Sims, Radiochim. Acta. **38**, 113 (1985).

[13] E. Browne and H. Junde, Nucl. Data Sheets **87**, 15 (1999).

[14] W.-T. Chou, W. A. Olivier, R. Aryaeinejad, Wm. C. McHarris, and O. Scholten, in *Proceedings of the Conference on High-Spin Nuclear Structure and Novel Nuclear Shapes, April 13-15, 1988, Argonne National Laboratory, Argonne, Illinois*; ANL-PHY, **88-2**, 292 (1988).

[15] Wm. C. McHarris, W.-T.C hou, and W. A. Olivier, Michigan State University Cyclotron Laboratory Annual Report No. 73, 1988 (unpublished).

[16] Y. H. Zhang *et al.*, Eur. Phys. J. A **7**, 19 (2000).

[17] Y. H. Zhang, S. Guo, X. H. Zhou, L. Ma, M. Oshima, Y. Toh, M. Koizumi, A. Osa, A. Kimura, Y. Hatsukawa, M. Sugawara, and H. Kusakari, Chin. Phys. Lett. **22**, 2788 (2005).

[18] Y. H. Zhang, S. Guo, X. H. Zhou, L. Ma, W. T. Guo, M. Oshima, Y. Toh, M. Koizumi, A. Osa, A. Kimura, Y. Hatsukawa, M. Sugawara, and H. Kusakari, Chin. Phys. Lett. **24**, 1203 (2006).

[19] M. Oshima *et al.*, J. Radioanal. Nucl. Chem. **278**, 257 (2008).

[20] T. Kibédi, G. D. Dracoulis, B. Fabricius, A. P. Byrne, and A. E. Stuchbery, Nucl. Phys. A **539**, 137 (1992).

[21] V. S. Shirley, Nucl. Data Sheets **75**, 377 (1995).

[22] A. Artna-Cohen, Nucl. Data Sheets **79**, 1 (1996).

[23] D. J. Hartley, W. H. Mohr, J. R. Vanhoy, M. A. Riley, A. Aguilar, C. Teal, R. V. F. Janssens, M. P. Carpenter, A. A. Hecht, T. Lauritsen, E. F. Moore, S. Zhu, F. G. Kondev, M. K. Djongolov, M. Danchev, L. L. Riedinger, G. B. Hagemann, G. Sletten, P. Chowdhury, S. K. Tandel, W. C. Ma, and S. W. Odegard, Phys. Rev. C **72**, 064325 (2005).

[24] K. S. Krane, R. M. Steffen, and R. M. Wheeler, Nucl. Data Tables **11**, 351 (1973).

[25] A. Krämer-Flecken, T. Morek, R. M. Lieder, W. Gast, G. Hebbinghaus, H. M. Jäger, and W. Urban, Nucl. Instrum. Methods Phys. Res. A **275**, 333 (1989).

[26] H. J. Jensen, R. A. Bark, P. O. Tjøm, G. B. Hagemann, I. G. Bearden, H. Carlsson, S. Leoni, T. Lonnroth, W. Reviol, L. L. Riedinger, H. Schnack-Petersen, T. Shizuma, X. Z. Wang, and J. Wrzesinski, Nucl. Phys. A **695**, 3 (2001).

[27] Nucl. Data Sheets **111**, viii (2010).

[28] K. S. Krane, Phys. Rev. C **8**, 1494 (1973).

[29] [http://www.nndc.bnl.gov/hsicc].

[30] R. A. Bark, A. M. Baxter, A. P. Byrne, P. M. Davidson, G. D. Dracoulis, S. M. Mullins, T. R. McGoram, and R. T. Newman, Phys. Rev. C **67**, 014320 (2003).

[31] C. J. Gallagher and S. A. Moszkowski, Phys. Rev. **111**, 1282 (1958).

[32] C. M. Baglin, Nucl. Data Sheets **109**, 2033 (2008).

[33] C. M. Baglin, Nucl. Data Sheets **96**, 399 (2002).

[34] M. Shamsuzzoha Basunia, Nucl. Data Sheets **102**, 719 (2004).

[35] F. G. Kondev, Nucl. Data Sheets **98**, 801 (2003).

[36] C. Thwaites, C. Wheldon, A. M. Bruce, P. M. Walker, G. D. Dracoulis, A. P. Byrne, T. Kibedi, F. G. Kondev, C. J. Pearson, and C. S. Purry, Phys. Rev. C **66**, 054309 (2002).

[37] C. J. Pearson, P. M. Walker, C. S. Purry, G. D. Dracoulis, S. Bayer, A. P. Byrne, T. Kibédi, and F. G. Kondev, Nucl. Phys. A **674**, 301 (2000).

[38] C. S. Purry, P. M. Walker, G. D. Dracoulis, S. Bayer, A. P. Byrne, T. Kibdi, F. G. Kondev, C. J. Pearson, J. A. Sheikh, and F. R. Xu, Nucl. Phys. A **672**, 54 (2000).

[39] A. K. Jain, R. K. Sheline, and D. M. Headly, Rev. Mod. Phys. **70**, 843 (1998).

[40] F. Donau and S. Frauendorf, in *Proceeding of the Conference on High Angular Momentum Properties of Nuclei, Oak Ridge*, 143, edited by N. R. Johnson (Harwood Academic, New York, 1982).

[41] G. D. Dracoulis, P. M. Walker, and A. Johnston, J. Phys. G **4**, 713 (1978).

[42] L. Hildingsson, W. Klamra, Th. Lindblad, C. G. Linden, C. A. Kalfas, S. Kossionides, C. T. Papadopoulos, R. Vlastou, J. Gizon, D. Clarke, F. Khazaie, and J. N. Mo, Nucl. Phys. A **513**, 394 (1990).

[43] P. M. Walker, G. D. Dracoulis, A. Johnston, J. R. Leigh, M. G. Slocombe, and I. F. Wright, J. Phys. G **4**, 1655 (1978).

[44] D. Hojman, M. A. Cardona, M. Davidson, M. E. Debray, A. J. Kreiner, F. Le Blanc, A. Burlon, J. Davidson, G. Levinton, H. Somacal, J. M. Kesque, F. Naab, M. Ozafrán, P. Stoliar, M. Vázquez, D. R. Napoli, D. Bazzacco, N. Blasi, S. M. Lenzi, G. Lo Bianco, and C. Rossi Alvarez, Phys. Rev. C **61**, 064322 (2000).

[45] M. Rudigier, J.-M. Régis, J. Jolie, K. O. Zell, and C. Fransen, Nucl. Phys. A **847**, 89 (2010).

[46] A. J. Kreiner, J. Davidson, M. Davidson, D. Abriola, C. Pomar, and P. Thieberger, Phys. Rev. C **36**, 2309 (1987).

[47] Y. Sun, S. X. Wen, and D. H. Feng, Phys. Rev. Lett. **72**, 3483 (1994).

[48] S.-X. Wen, H. Z., S.-G. Li, G.-S. Li, G.-J. Yuan, P.-F. Hua, P.-K. Weng, L.-K. Zhang, P.-S. Yu, C.-X. Yang, H.-B. Sun, Y.-B. Liu, Y.-Z. Liu, Y. Sun, and D. H. Feng, Phys. Rev. C **54**, 1015 (1996).

[49] H. M. El-Masri, P. M. Walker, G. D. Dracoulis, T. Kibedi, A. P. Byrne, A. M. Bruce, J. N. Orce, A. Emmanouilidis, D. M. Cullen, C. Wheldon, and F. R. Xu, Phys. Rev. C **72**, 054306 (2005).

[50] S. K. Tandel, P. Chowdhury, E. H. Seabury, I. Ahmad, M. P. Carpenter, S. M. Fischer, R. V. F. Janssens, T. L. Khoo, T. Lauritsen, C. J. Lister, D. Seweryniak, and Y. R. Shimizu, Phys. Rev. C **73**, 044306 (2006).

[51] A. J. Kreiner, M. A. J. Mariscotti, C. Baktash, E. der Mateosian, and P. Thieberger, Phys. Rev. C **23**, 748 (1981).

[52] F. R. Xu, W. Satula, and R. Wyss, Nucl. Phys. A **669**, 119 (2000).

[53] H. J. Jensen, G. B. Hagemann, P. O. Tjøm, S. Frauendorf, A. Atac, M. Bergström, A. Bracco, A. Brockstedt, H. Carlsson, P. Ekström, J. M. Espino, B. Herskind, F. Ingebretsen, J. Jongman, S. Leoni, R. M. Lieder, T. Lönnroth, A. Maj, B. Million, A. Nordlund, J. Nyberg, M. Piiparinen, H. Ryde, M. Sugawara, and A. Virtanen, Z. Phys. A **340**, 351 (1991).

[54] W. Nazarewicz, G. A. Leander, and J. Dudek, Nucl. Phys. A **467**, 437 (1987).

[55] R. Wyss, J. Nyberg, A. Johnson, R. Bengtsson, and W. Nazarewicz, Phys. Lett. B **215**, 211 (1988)

[56] W. Nazarewicz, R. Wyss, and A. Johnson, Nucl. Phys. A **503**, 285 (1989).

[57] Zs. Podolyak, S. Al-Garni, R. F. Casten, J. R. Cooper, D. M. Cullen, A. Dewald, R. Krucken, H. Newman, J. N. Orce, C. J. Pearson, C. Ur, R. Venturelli, S. Vincent, C. Wheldon, P. M. Walker, F. R. Xu, A. Yamamoto, and N. V. Zamfir, Phys. Rev. C **66**, 011304 (2002).

[58] W. Nazarewicz, J. Dudek, R. Bengtsson, T. Bengtsson, and I. Ragnarsson, Nucl. Phys. A **435**, 397 (1985).

[59] S. K. Chamoli *et al.*, Phys. Rev. C **66**, 024307 (2002).